

NUMERICAL STUDY OF THE BLOCKAGE EFFECTS ON VISCOUS FLOW PAST A CIRCULAR CYLINDER

P. ANAGNOSTOPOULOS AND G. ILIADIS

Department of Civil Engineering, Aristotle University of Thessaloniki, Thessaloniki 54006, Greece

AND

S. RICHARDSON

Department of Aeronautics, Imperial College of Science Technology and Medicine, London SW7 2BY, U.K.

SUMMARY

In various numerical solutions of flow around bluff bodies the unbounded physical domain is replaced by a restricted computational one whose extent depends on the size of the computational grid network. The truncation of the solution domain in the cross-flow direction reduces the computer time required for the solution, but introduces numerical blockage effects which influence considerably the values of the various flow parameters. In the present paper the finite element solution of steady and unsteady flow around a circular cylinder at $Re = 106$ is presented for blockage ratios of 0.05, 0.15 and 0.25. A boundary condition was tested for which the streamfunction values at the outer boundaries were those of the irrotational solution around a circular cylinder. The size of the standing vortices decreases with the blockage ratio when the flow is steady, while the spacing of the vortices decreases in both directions with increasing blockage ratio when the wake becomes unsteady. The hydrodynamic forces on the cylinder and the Strouhal number are magnified as the blockage ratio increases. The application of the streamfunction values derived from the irrotational solution at the outer boundaries reduced blockage effects only at high blockage ratio.

KEY WORDS: vortex shedding; blockage; Strouhal number; drag force; lift force

INTRODUCTION

One of the most popular aspects of computational fluid dynamics is the numerical solution of flow around bluff bodies. Although considerable attention has been given to other cross-sections, most of the work carried out is related to flow around a circular cylinder. It has long been known that steady symmetrical flow behind the cylinder occurs for Reynolds numbers extending up to approximately 50. For higher values of Re the wake behind the cylinder becomes unsteady and a periodic wake of staggered vortices is observed, known as 'von Kármán vortex street'. The unsteady wake behind the cylinder is fully laminar when the Reynolds number lies between 50 and 150, which is referred to as the 'stable range'. When flow around one half of the cylinder is considered or a splitter plate of adequate length is placed behind the cylinder on the wake centreline, the steady symmetrical flow persists for Reynolds numbers higher than 50.

With the advent and continuous increase in power of digital computers, numerical solutions of flow around a cylinder in the laminar regime started to emerge. Jain and Rao,¹ Thoman and Szweczyk,² Son and Hanratty³ and Dennis and Chang⁴ presented finite difference solutions of steady flow around a circular cylinder. Jordan and Fromm,⁵ Swanson and Spaulding⁶ and Franke *et al.*⁷ used the finite difference technique for the solution of the vortex shedding behind a cylinder. Taylor and Hood⁸ and

Tuann and Olson⁹ employed the finite element method for the solution of steady flow around a circular cylinder, while Smith and Brebbia,¹⁰ Gresho *et al.*,¹¹ Eaton,¹² Karniadakis and Triantafyllou¹³ and Anagnostopoulos¹⁴ presented solutions of the vortex street wake.

Numerical solutions provide a complete description of the field variables throughout the solution domain, whose measurement with an experimental technique at a large number of points in the flow field is usually a difficult if not formidable task. On the other hand, their accuracy depends on many factors, such as the numerical technique used and the refinement of the computational grid. Moreover, when the flow around a body is examined experimentally, the flow field is practically unbounded in most cases, whereas in a numerical solution external boundaries are imposed, whose distance from the body depends on the extent of the computational mesh. The proximity of the external boundaries to the cylinder reduces the size of the computational mesh and the computer time required for the solution, but induces numerical blockage which alters the flow characteristics. In many cases no information about the computational mesh is given, so no assessment of the effect of the numerical blockage on the results can be made. Chilukuri¹⁵ investigated the blockage effect on the flow past a fixed and transversely vibrating cylinder using four different finite difference grids. Karniadakis and Triantafyllou¹³ found with a spectral element technique that a substantial decrease in the blockage ratio has an effect a small reduction of the Strouhal number at $Re = 100$. Ren and Utnes¹⁶ used two different meshes for the solution of flow around a cylinder at $Re = 175$. They report higher absolute value pressures around the cylinder for greater blockage ratio, whereas the coarser mesh causes delay of vortex shedding. Stansby and Slaouti¹⁷ investigated the blockage effects on the periodic wake behind a circular cylinder at Re between 60 and 180 using the random vortex method. Anagnostopoulos¹⁸ examined the flow around a fixed and vortex-excited cylinder oscillating in the cross-flow direction at Re around 100 using the finite element technique. The computational results were to be compared with experimental data under similar conditions in a water channel of large cross-sectional area. Owing to the great distance of the channel walls from the cylinder, the physical flow phenomenon was practically unbounded, while the blockage ratio of the computational mesh was 15 per cent. It had been found experimentally¹⁹ that even a small fluctuation of the Reynolds number had as effect a significant change in the cylinder oscillation amplitude at steady state. Therefore blockage correction formulae were used for the comparison of results, which had been used previously²⁰ for the correction of experimental results at much higher Reynolds numbers. For the validation of the applicability of these formulae in this low-Reynolds-number regime, computations with meshes of lower blockage ratio were also made.

In the present investigation the blockage effect on the steady and unsteady wake of a circular cylinder will be examined numerically at Reynolds number equal to 106 using the finite element technique. Particular attention will be given to the flow pattern and the hydrodynamic forces exerted on the cylinder.

SOLUTION TECHNIQUE

The mathematical model of the problem consists of the Navier–Stokes equations in the formulation where the streamfunction Ψ and the vorticity ζ are the field variables. Considering the values of Ψ and ζ at two successive time steps n and $n + 1$, the governing equations become

$$\nabla^2 \Psi_{n+1} = -\zeta_n, \quad (1)$$

$$\frac{\partial \zeta_{n+1}}{\partial t} + \frac{\partial \Psi_{n+1}}{\partial y} \frac{\partial \zeta_n}{\partial x} - \frac{\partial \Psi_{n+1}}{\partial x} \frac{\partial \zeta_n}{\partial y} = \nu \nabla^2 \zeta_{n+1}. \quad (2)$$

The vorticity is evaluated at point A on the cylinder surface by

$$\zeta_A = \frac{3}{\Delta\eta^2}(\Psi_A - \Psi_B) - \frac{\zeta_B}{2}, \tag{3}$$

where point B lies on the normal to the cylinder through A and $\Delta\eta$ is the distance between points A and B.

Applying the Galerkin method to equations (1) and (2) for each element and assembling for the whole continuum, we obtain

$$[K_1]\{\Psi\}_{n+1} = [K_2]\{\zeta\}_n + \{R_1\}, \tag{4}$$

$$[K_3]\{\zeta\}_{n+1} + [K_4]\{\dot{\zeta}\}_{n+1} + \{R_2\} = \{R_3\}, \tag{5}$$

where $[K_1]$, $[K_2]$, $[K_3]$ and $[K_4]$ are square matrices stored in banded form and $\{R_1\}$, $\{R_2\}$ and $\{R_3\}$ are column matrices. If $\partial\Psi/\partial\eta = 0$ and $\partial\zeta/\partial\eta = 0$ throughout the boundaries where a natural boundary condition is imposed, $\{R_1\}$ and $\{R_3\}$ are zero.

The boundary conditions are depicted in Figure 1. The vorticity was taken equal to zero throughout the outer boundary, except for the outflow boundary where the boundary condition $\partial\zeta/\partial\eta$ was used. Two different boundary conditions were tested for the streamfunction. The first, shown in Figure 1(b), dictates constant streamfunction along the upper and lower boundaries, a situation equivalent to flow through a frictionless channel. The second, displayed in Figure 1(c), is based on irrotational flow around a circular cylinder, where the streamlines are displaced outwards near the cylinder. The streamfunction is not constant along the upper and lower boundaries, because the points of these boundaries belong to different streamlines. The boundary condition $\partial\Psi/\partial\eta$ was imposed at the outflow boundary. The solution algorithm consists of the following steps.

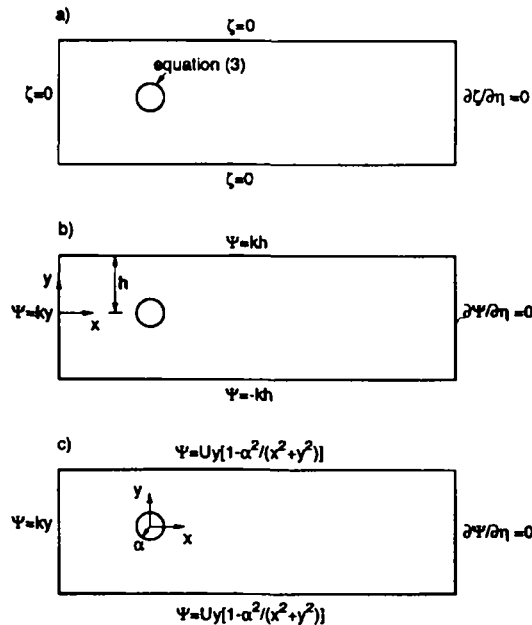


Figure 1. Boundary conditions: (a) vorticity; (b) streamfunction; (c) streamfunction from irrotational solution at outer boundaries.

- (a) The streamfunction is evaluated at time $t + \Delta t$ from equation (4). The values of vorticities are those calculated in the previous time step or, in particular, the initial conditions.
- (b) The vorticity values at the no-slip boundary are corrected from equation (3).
- (c) The vorticities at time $t + \Delta t$ are calculated from equation (5).

The pressure distribution throughout the flow field was calculated from the Poisson equation

$$\frac{\partial^2 P}{\partial x^2} + \frac{\partial^2 P}{\partial y^2} = -2\rho \left(\frac{\partial u}{\partial y} \frac{\partial v}{\partial x} - \frac{\partial u}{\partial x} \frac{\partial v}{\partial y} \right), \quad (6)$$

which is solved in the same way as equation (1). The shear stress on the cylinder can be calculated from

$$\tau_w = \mu \zeta_w. \quad (7)$$

From the integration of shear stress and pressure distribution around the cylinder the shear and pressure forces on the cylinder were derived. Next the in-line and transverse components of these forces were evaluated.

Three computational meshes with different blockage ratios were used for the investigation of the blockage effect. All of them are of the same shape and are based on the equipotential lines for irrotational flow past a circular cylinder. The mesh depicted in Figure 2 contains 6460 nodes and 12552 elements, the blockage ratio being 0.05. The mesh of Figure 3 contains 3639 nodes and 6960 elements and has blockage ratio 0.15, while the mesh of Figure 4 used for the investigation of blockage ratio 0.25 contains 2701 nodes and 5118 elements. The distance between the outflow boundary and the cylinder centre was approximately 20 cylinder diameters.

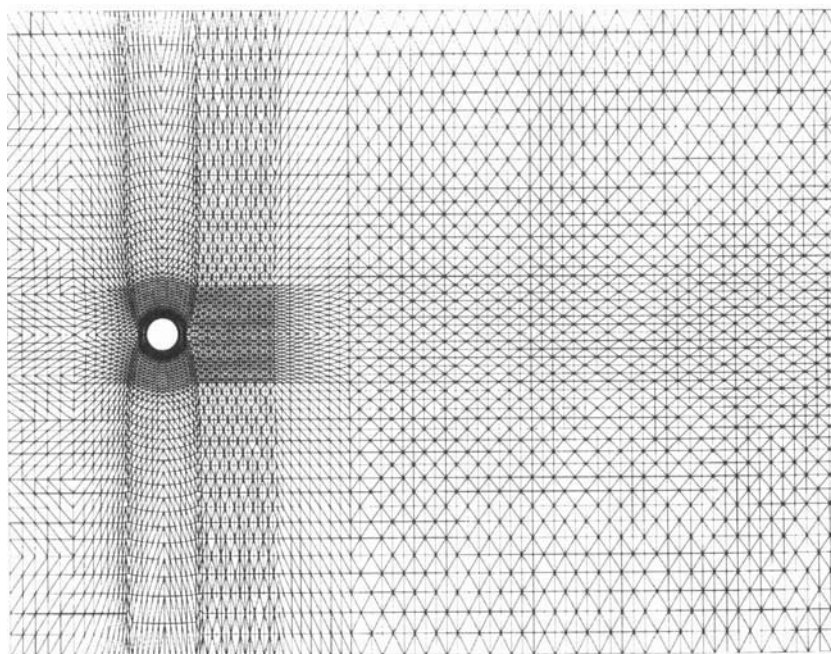


Figure 2. Finite element mesh for blockage ratio 0.05

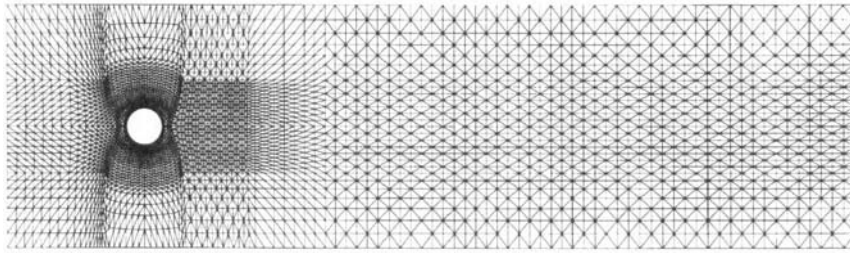


Figure 3. Finite element mesh for blockage ratio 0.15

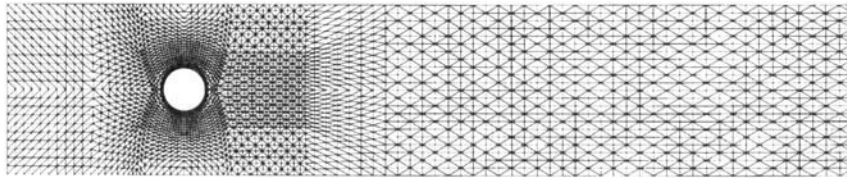


Figure 4. Finite element mesh for blockage ratio 0.25

APPLICATION RESULTS

The same solution procedure was used for all three computational meshes depicted in Figures 2–4. For blockage ratios 0.15 and 0.25 the solution was performed with both boundary conditions for the streamfunction shown in Figures 1(b) and 1(c). The solution started assuming zero vorticity throughout the flow field. As time increases, a pair of standing vortices is formed behind the cylinder, growing continually in size. When the vortices have increased considerably, small asymmetries due to round-off errors are detectable, which eventually lead to the formation of the unsteady wake known as the ‘von Kármán vortex street’. Since one of the aims of the project was the investigation of blockage on the wake for symmetric flow, the symmetry across the wake centreline was forced by eliminating artificially these asymmetries until the size of the vortices was stabilized. The streamlines for all three blockage ratios are depicted in Figure 5. At high blockage ratios the proximity of the channel walls suppresses the vortices formed behind the cylinder and reduces the wake length. The separating streamline crosses the wake centreline at a distance equal to 6.2 cylinder diameters from the trailing edge of the cylinder for $d/h = 0.05$, 5 diameters for $d/h = 0.15$ and 4.3 diameters for $d/h = 0.25$. The wake length for $d/h = 0.05$ computed herein agrees considerably with the values of previous investigations quoted by Tuann and Olson.⁹ The dimensionless pressure distribution $C_p = p/0.5\rho U^2$ around the cylinder for the three blockage ratios is presented in Figure 6. The absolute values of pressure increase significantly with the blockage ratio, whereas the pressure at the trailing edge is the same for all cases. A point of great interest is the significant increase in the stagnation pressure with the blockage ratio. The dimensionless vorticity distribution $\zeta^* = \zeta d/2U$ around the cylinder is depicted in Figure 7. Figure 7 indicates an increase in vorticity around the cylinder with the blockage ratio. The effect of the boundary condition on the pressure distribution around the cylinder for $d/h = 0.25$ is presented in Figure 8. Figure 8 reveals that the application of the ‘irrotational’ boundary condition reduces the absolute values of the pressures around the cylinder for $d/h = 0.25$, while the application of the same boundary condition has no significant effect on the pressure distribution for the other blockage ratios. The values of the basic flow parameters for the standing vortex case for the three blockage ratios examined are summarized in Table

I. The 'irrotational' boundary condition for the streamfunction on the external boundaries is denoted with 'lr.' after the number corresponding to the blockage ratio examined.

Table I reveals that the drag coefficient increases with the blockage ratio, whereas the irrotational boundary condition has as effect the decrease in the drag coefficient with respect to the constant streamfunction value. These results are compatible with the pressure distributions shown in Figures 6 and 8. The separation angle increases with the blockage ratio, while the application of the irrotational boundary condition yields higher separation angles.

The round-off errors lead to asymmetries which are amplified gradually until the wake becomes fully periodic. The time history of the drag coefficient is depicted for $d/h = 0.05$ in Figure 9 and for $d/h = 0.25$ in Figure 10. The basic features of the two figures are similar. After a sudden increase in the drag immediately after the impulsive start of the phenomenon, the drag coefficient decreases gradually, tending asymptotically to the value quoted in Table I, which corresponds to symmetric flow. Then, owing to asymmetries associated with round-off errors, the drag increases until the vortex street is fully

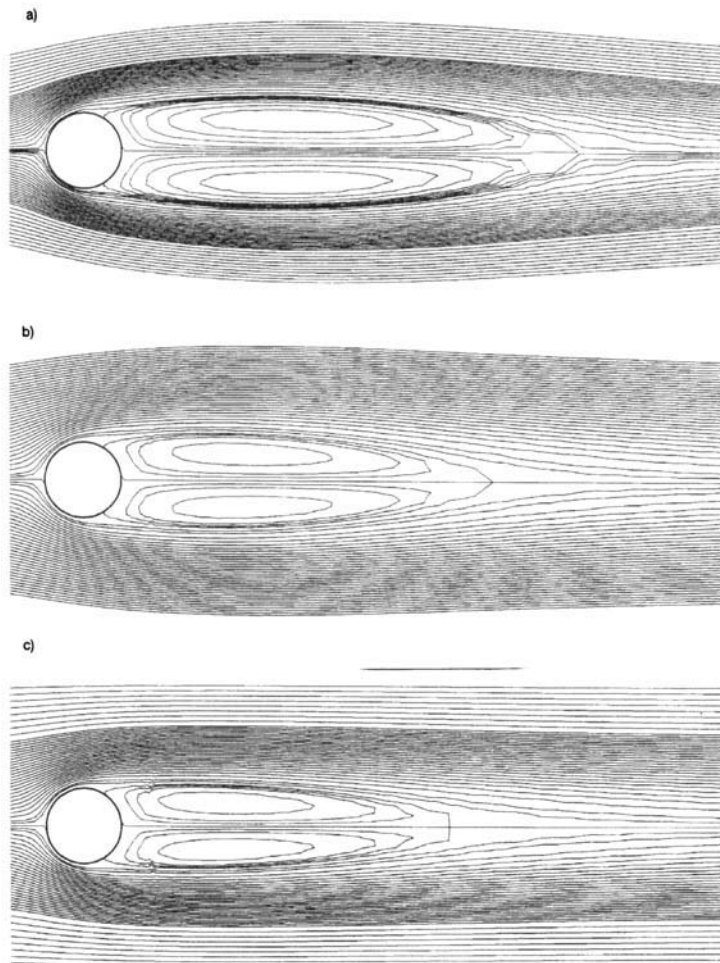


Figure 5. Streamlines for steady flow: (a) $d/h = 0.05$; (b) $d/h = 0.15$; (c) $d/h = 0.25$

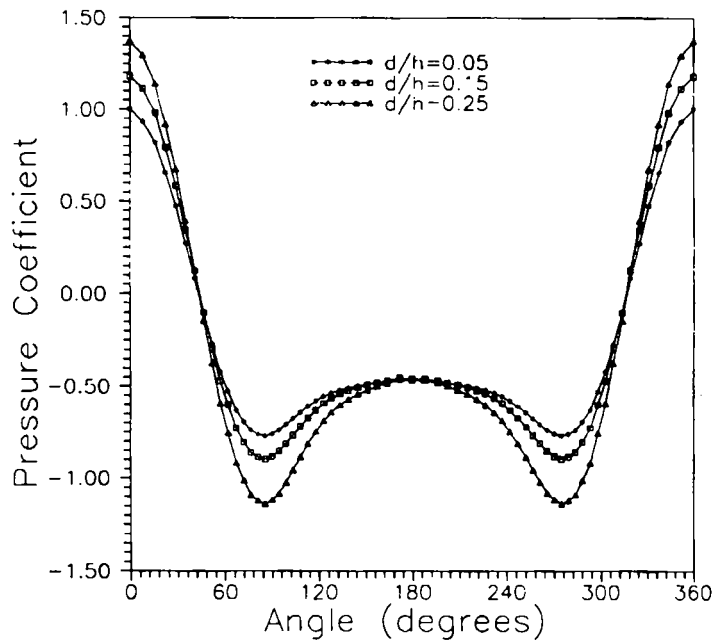


Figure 6. Pressure distribution around cylinder for three blockage ratios

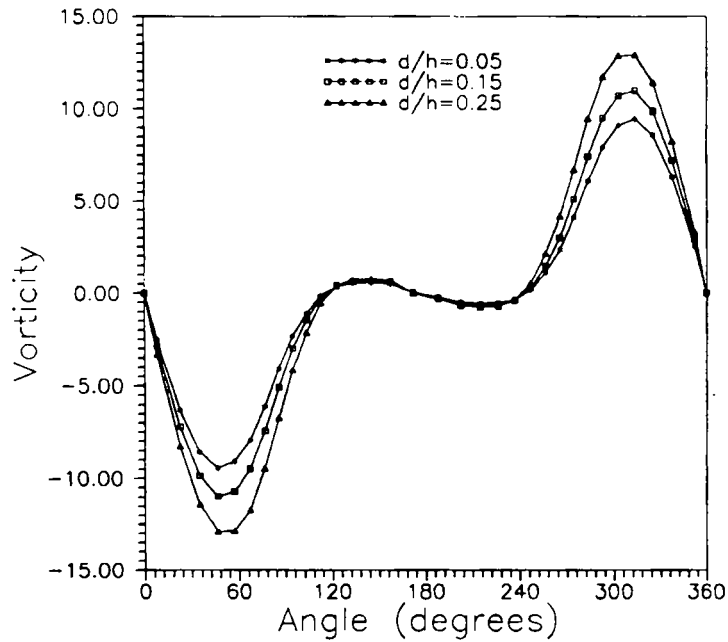


Figure 7. Vorticity distribution around cylinder for three blockage ratios

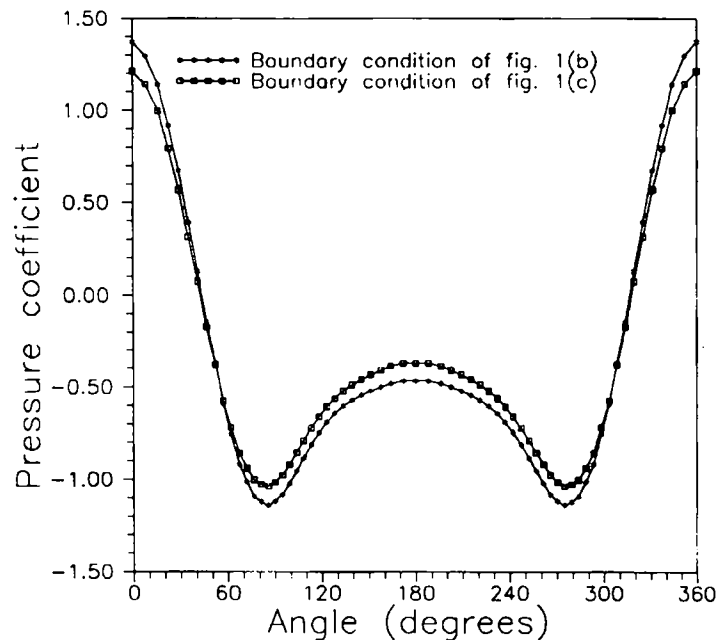


Figure 8. Effect of boundary condition on pressure distribution around cylinder; $d/h = 0.25$

Table I. Effect of blockage ratio on flow parameters of symmetric flow behind cylinder

Blockage ratio	Drag coefficient	Pressure drag	Separation angle (deg)	Wake length (diameters)
0.05	1.075	0.804	115.87	6.2
0.15	1.229	0.907	116.94	5.0
0.15 lr.	1.219	0.899	117.14	5.0
0.25	1.416	1.019	118.66	4.3
0.25 lr.	1.343	0.967	119.31	4.3

established. The differences between Figures 9 and 10 are that (i) at $d/h = 0.05$ the asymmetries in the wake manifested by the increase in drag appear before the full size of the standing vortices develops, contrary to the case when $d/h = 0.25$, and (ii) at $d/h = 0.05$ a peak appears in the mean drag at $t = 2$ s and then a slow decrease to the steady state value, which is not the case at $d/h = 0.25$. The lift coefficient on the cylinder as a function of time is depicted for $d/h = 0.05$ in Figure 11 and for $d/h = 0.025$ in Figure 12. The lift amplitude when $d/h = 0.05$ displays a peak at $t = 1.9$ and then decreases to the steady state value. On the other hand, when $d/h = 0.25$, the lift amplitude increases continually to the constant value. The separation angles are depicted in Figure 13 for $d/h = 0.05$ and in Figure 14 for $d/h = 0.25$. The separation angle decreases abruptly as the size of the standing vortices increases after the impulsive start of the phenomenon. A peak is detectable in Figure 13 at $t = 1.9$ as in the lift and drag forces, while the separation angle at each side of the cylinder becomes maximum when that at the other side becomes minimum and vice versa. When $d/h = 0.15$, the time histories of drag, lift and separation angles are similar to those at $d/h = 0.25$, without the intermediate peaks present at $d/h = 0.05$. The equivorticity lines for the three blockage ratios when the lift force on the cylinder becomes maximum are depicted in

Figure 15. At $d/h = 0.25$ the vortices are suppressed in the cross-flow direction, acquiring a rounder shape than at lower blockage ratios. At the same blockage ratio the outermost vorticity contours are in contact with the walls of the channel. The pressure distribution around the cylinder when the lift force becomes maximum is depicted in Figure 16. The pressure difference at the two opposite sides of the cylinder increases with the blockage ratio, giving rise to a higher lift force. The characteristics of the unsteady wake for the three blockage ratios are summarized in Table II.

Table II reveals that when the blockage ratio increases, the longitudinal and lateral spacings α and β decrease in such a way that the spacing ratio β/α remains almost constant, close to 0.281, the value of the von Kármán analysis. The high blockage ratio increases the Strouhal number. The separation angle increases with the blockage ratio, whereas the irrotational boundary condition has an effect the further increase in the separation angles. The forces exerted on the cylinder for the three blockage ratios considered are summarized in Table III.

Table III shows again that the hydrodynamic forces on the cylinder increase considerably with the blockage ratio. The mean drag increases by 20 per cent when the blockage ratio is increased from 5 per cent to 25 per cent, while the lift amplitude is almost doubled. The application of the irrotational boundary condition reduces the hydrodynamic forces on the cylinder, with more spectacular reduction of the lift force. Therefore the blockage ratio is an important parameter when the hydrodynamic forces around a body are derived computationally and its effects should be seriously considered. Stansby and Slaouti¹⁷ quote similar values of the Strouhal number for the same blockage ratio. The drag coefficient found by the same investigators at low blockage is very close to that of the present solution, but the blockage effect is higher in their solution. Smaller agreement is observed in the lift coefficient, whose values calculated herein are substantially lower than the values given by Stansby and Slaouti.¹⁷ The lift amplitude coefficient is the quantity mostly dependent on the solution technique, with serious scatter of results obtained from different solutions. Smith and Brebbia¹⁰ report high deviations of the lift coefficient, depending on the time integration scheme and the 'lumping' of the mass in the coefficient matrices, with reduction of the computational time. The only experimental value for the lift amplitude existing in the literature to the authors' knowledge in this range of Reynolds numbers is that by Tanida *et*

Table II. Effect of blockage ratio on vortex street parameters behind cylinder

Blockage ratio	α/d	β/d	β/α	Strouhal number	Separation angle (deg)
0.05	5.437	1.44	0.264	0.1658	117.73–120.34
0.15	4.875	1.25	0.256	0.1907	117.74–120.84
0.15 lr.	5.111	1.33	0.260	0.1893	117.87–120.84
0.25	4.450	1.18	0.265	0.2239	118.58–121.58
0.25 lr.	4.777	1.11	0.233	0.2192	119.18–121.77

Table III. Hydrodynamic forces on cylinder for various blockage ratios in vortex-shedding case

Blockage ratio	Mean drag coefficient	Pressure drag	Drag fluctuation peak to peak	Lift amplitude
0.05	1.284	0.972	0.0135	0.165
0.15	1.438	1.087	0.0216	0.256
0.15 lr.	1.413	1.065	0.0205	0.242
0.25	1.661	1.247	0.0310	0.315
0.25 lr.	1.529	1.140	0.0225	0.256

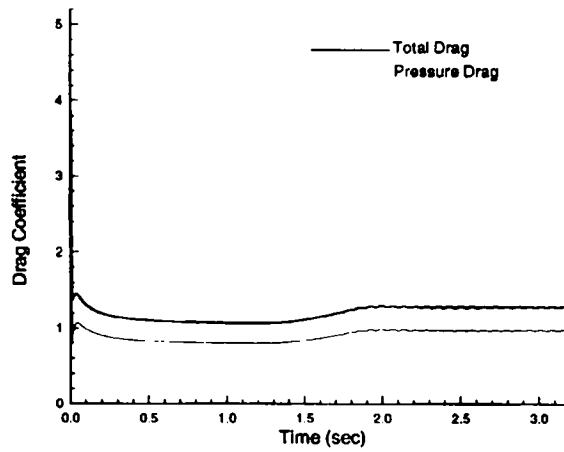


Figure 9. Time history of drag coefficient; $d/h = 0.05$

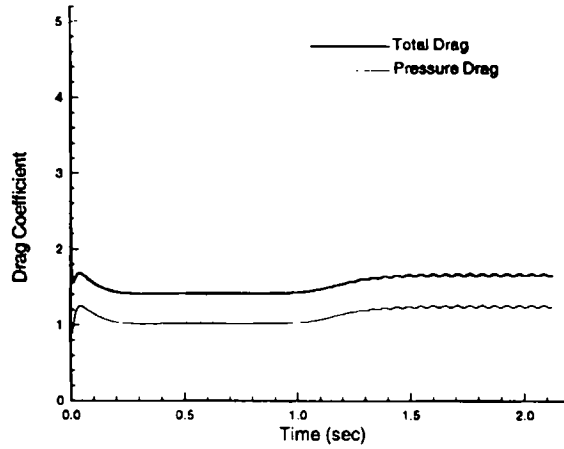


Figure 10. Time history of drag coefficient; $d/h = 0.25$

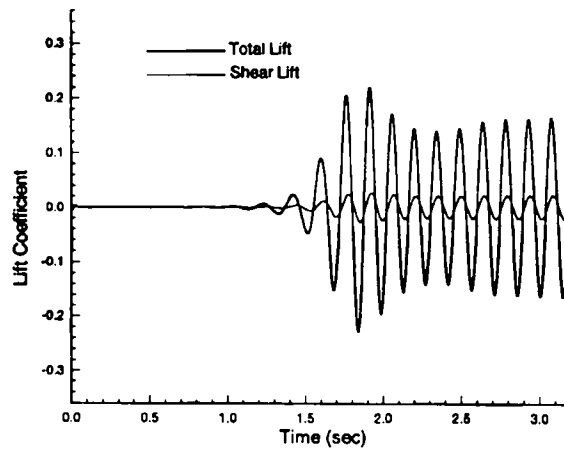


Figure 11. Time-dependent lift coefficient on cylinder; $d/h = 0.05$

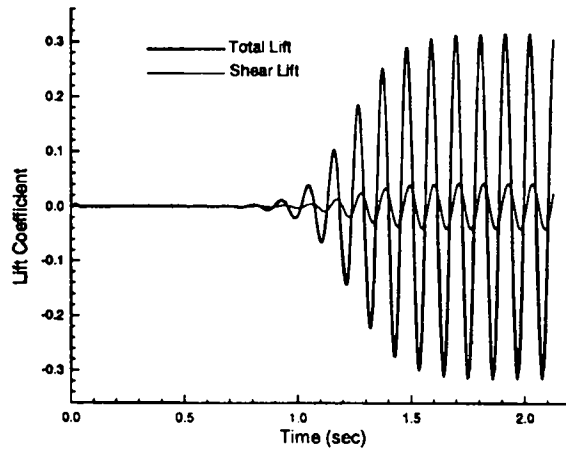


Figure 12. Time-dependent lift coefficient on cylinder; $d/h = 0.25$

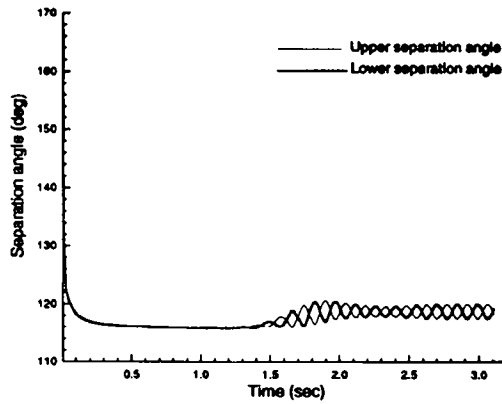


Figure 13. Separation angles as functions of time; $d/h = 0.05$

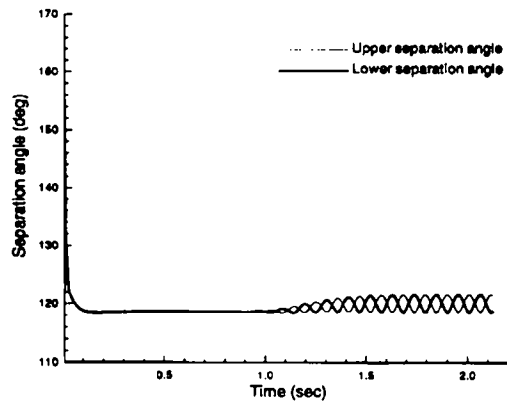


Figure 14. Separation angles as functions of time; $d/h = 0.25$

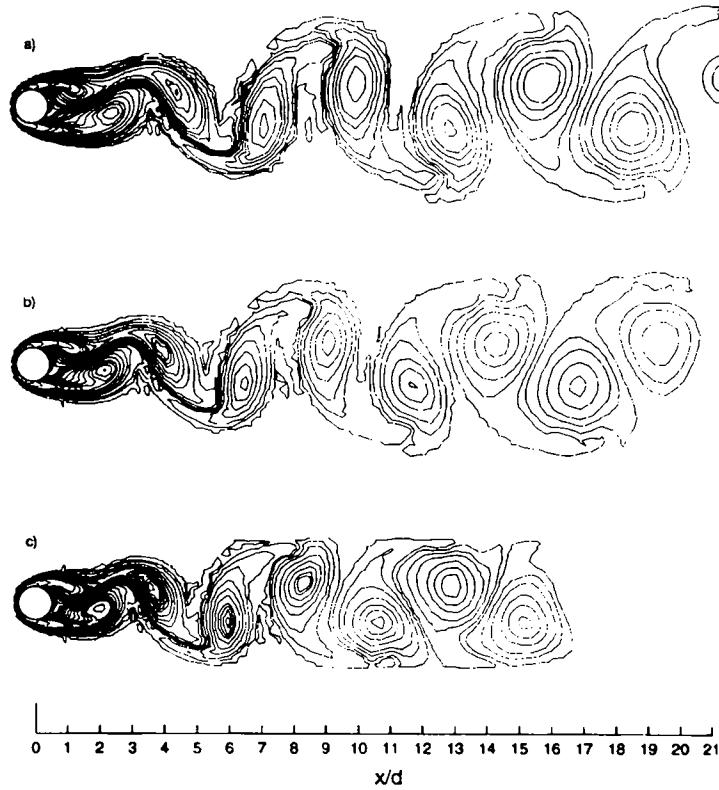


Figure 15. Equivorticity lines for unsteady flow: (a) $d/h = 0.05$; (b) $d/h = 0.15$; (c) $d/h = 0.25$

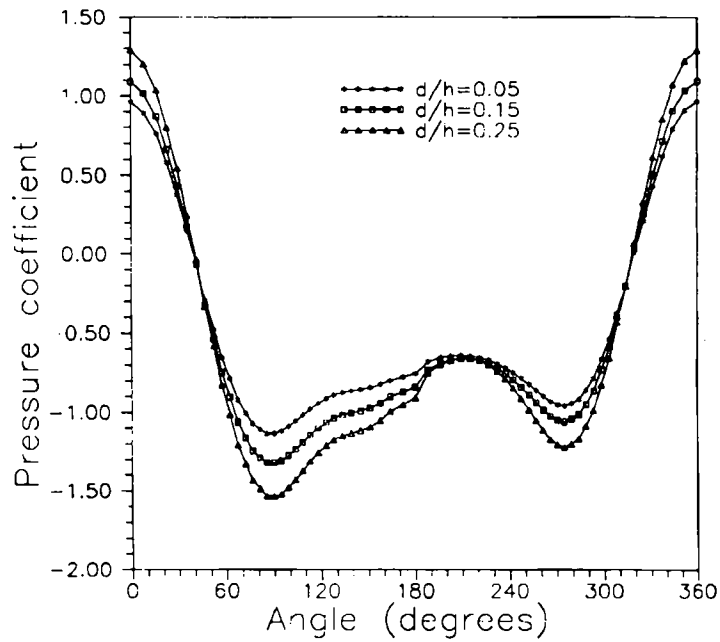


Figure 16. Pressure distribution around cylinder for unsteady flow

al.,²¹ who used strain gauges for the measurement of the lift force. They report for $Re = 100$ a value equal to 0.0875, which is substantially lower than the values derived computationally. In spite of the fact that the experimental value is expected to be lower than that of a two-dimensional computation owing to the oblique shedding of vortices along the span, there exists uncertainty about the accuracy of this result because of the difficulty of measurement of a force of so small a scale.

Each computer cycle required 10.2 CPU seconds on the VAX 9000 computer of the University of Thessaloniki for the mesh of Figure 2, 6.9 s for the mesh of Figure 3 and 3.5 s for the mesh of Figure 4. At each time step, three systems of equations were solved.

CONCLUSIONS

The finite element technique was used for the solution of steady and unsteady flow around a circular cylinder at $Re = 106$ for blockage ratios of 0.05, 0.15 and 0.25. When the flow remains steady in the form of two standing vortices behind the cylinder, the size of the vortices is reduced considerably as the blockage ratio increases. Moreover, the drag force and the separation angle increase with the blockage ratio.

When a vortex street wake is formed behind the cylinder, the longitudinal and lateral spacings of the vortices decrease as the blockage ratio increases, in such a way that their ratio remains almost constant. The Strouhal number, separation angles and hydrodynamic forces increase with the blockage ratio. The most prominent effect of blockage is on the amplitude of the fluctuating lift force, which increases by 90 per cent as the blockage ratio is increased from 0.05 to 0.25. The application of the streamfunction values derived from the irrotational solution around a circular cylinder at the external boundaries reduced the blockage effects for blockage ratio 0.25 but did not alter the results considerably for blockage ratio 0.15.

Therefore blockage effects are significant for the accuracy of the results of a numerical solution. When meshes with high blockage ratios are used for the reduction of computational time required, the values of the various hydrodynamic parameters may be considerably different from those of an unbounded solution.

REFERENCES

1. P. C. Jain and K. S. Rao, 'Numerical solution of unsteady viscous incompressible fluid flow past a circular cylinder', *Phys. Fluids Suppl. II*, 57-64 (1969).
2. D. C. Thoman and A. A. Szewczyk, 'Time-dependent viscous flow over a circular cylinder', *Phys. Fluids Suppl. II*, 76-86 (1969).
3. J. S. Son and T. J. Hanratty, 'Numerical solution for the fluid flow around a cylinder at Reynolds numbers of 40, 200 and 500', *J. Fluid Mech.*, **35**, 369-386 (1969).
4. S. C. R. Dennis and G. Chang, 'Numerical solutions for steady flow past a circular cylinder at Reynolds numbers up to 100', *J. Fluid Mech.*, **42**, 471-489 (1970).
5. S. K. Jordan and J. E. Fromm, 'Oscillatory drag, lift, and torque on a circular cylinder in a uniform flow', *Phys. Fluids*, **15**, 371-376 (1972).
6. J. C. Swanson and M. L. Spaulding, 'Three dimensional numerical model of vortex shedding from a circular cylinder', *Proc. ASME Symp. on Non-steady Fluid Dynamics*, ASME, New York, 1978, pp. 207-216.
7. R. Franke, W. Rodi and B. Schoenung, 'Numerical calculation of laminar vortex-shedding flow past cylinders', *J. Wind Eng. Ind. Aerodyn.*, **35**, 237-257 (1990).
8. C. Taylor and P. Hood, 'A numerical solution of the Navier-Stokes equations using the finite element method', *Comput. Fluids*, **1**, 73-100 (1973).
9. S. Tuann and M. D. Olson, 'Numerical studies of the flow around a circular cylinder by a finite element method', *Comput. Fluids*, **6**, 219-240 (1978).
10. S. L. Smith and C. A. Brebbia, 'Improved stability techniques for the solution of Navier-Stokes equations', *Appl. Math. Model.*, **1**, 226-234 (1977).
11. P. M. Gresho, R. L. Lee and R. L. Sani, 'On the time-dependent solution of the incompressible Navier-Stokes equations in two and three dimensions', in C. Taylor and K. Morgan (eds), *Recent Advances in Numerical Methods in Fluids*, Pineridge, Swansea, 1980, pp. 27-79.

12. B. E. Eaton, 'Analysis of laminar vortex shedding behind a circular cylinder by computer-aided flow visualization', *J. Fluid Mech.*, **180**, 117–145 (1987).
13. G. E. Karniadakis and G. S. Triantafyllou, 'Three-dimensional dynamics and transition to turbulence in the wake of bluff bodies', *J. Fluid Mech.*, **238**, 1–30 (1992).
14. P. Anagnostopoulos, 'Numerical solution for laminar two-dimensional flow about a fixed and transversely oscillating cylinder in a uniform stream', *J. Comput. Phys.*, **85**, 434–456 (1989).
15. R. Chilukuri, 'Incompressible laminar flow past a transversely vibrating cylinder', *ASME J. Fluids Eng.*, **109**, 166–171 (1987).
16. G. Ren and T. Umes, 'A finite element solution of the time-dependent incompressible Navier–Stokes equations using a modified velocity correction method', *Int. j. numer. methods fluids*, **17**, 349–364 (1993).
17. P. K. Stansby and A. Slaouti, 'Simulation of vortex shedding including blockage by the random-vortex and other methods', *Int. j. numer. methods fluids*, **17**, 1003–1013 (1993).
18. P. Anagnostopoulos, 'Numerical investigation of response and wake characteristics of a vortex-excited cylinder in a uniform stream', *J. Fluids Struct.*, **8**, 367–390 (1994).
19. P. Anagnostopoulos and P. W. Bearman, 'Response characteristics of a vortex-excited cylinder at low Reynolds numbers', *J. Fluid Struct.*, **6**, 39–50 (1992).
20. A. Roshko, 'Experiments on the flow past a circular cylinder at very high Reynolds number', *J. Fluid Mech.*, **10**, 345–356 (1961).
21. Y. Tanida, A. Okajima and Y. Watanabe, 'Stability of a circular cylinder oscillating in uniform flow or in a wake', *J. Fluid Mech.*, **61**, 769–784 (1973).